Journal of Coastal Research	6	4	927-942	Fort Lauderdale, Florida	Fall 1990

Spatial Variation in Sinusoidal Wave Energy on a Crescentic Nearshore Bar; Application to the Cap-Ferret Coast, France

Jean-Marie Froidefond, Jean-Marie Gallissaires and Robert Prud'Homme

Departement de Géologie et Océanographie
Université de Bordeaux I
C.N.R.S., U.A. 197
Avenue des Facultés
33405 Talence cedex, France

ABSTRACT

FROIDEFOND, J.-M.; GALLISSAIRES, J.-M., and PRUD'HOMME, R., 1990. Spatial variation in sinusoidal wave energy on a crescentic nearshore bar: Application to the Cap-Ferret coast, France. *Journal of Coastal Research*, 6(4), 927-942. Fort Lauderdale (Florida). ISSN 0749-0208.

Simple sinusoidal wave refraction on a crescentic bar off the Aquitaine coast has been studied. In the case of parallel waves to the coast, this bar, composed of a cyclical repetition of troughs separated by ridges, induces a synchronous variation in wave height and energy flux along the shore. Energy flux is lower in the troughs than on the ridges. The longshore component of energy flux changes more rapidly than the total flux. The theoretical distribution of this energy is analyzed in comparison with the water depth changing in accordance with the tide. The results show a variation in the longshore component and thus a displacement of circulation cells and rip-currents during the course of the tide. In the case of oblique waves to the coast, the cyclic variation of energy flux decreases and the longshore component increases. The rip-currents are unwedged by comparison with the previous case. These results are compared with aerial photographs. A second crescentic bar and tidal channels complicate the refraction process.

ADDITIONAL INDEX WORDS: *Crescentic bars, energy flux, parallel waves, refraction process, rip currents, tidal channel, French coast.*

INTRODUCTION

Crescentic bars characterize many sandy coasts such as those of the coast of Southeastern Australia, the coasts of Florida and North Carolina, the Algerian coast, the Israeli coast, the Gulf of Lion and the Aquitaine coasts in France, for example. Studies have been published on their morphology (*e.g.* HOM-MA and SONU, 1963; GREENWOOD and DAVIDSON-ARNOTT, 1975; BARRUSSEAU and SAINT-GUILY, 1981; GOLDSMITH *et al.*, 1982) and hypotheses put forward for formation (*e.g.* CLOS-ARCEDUC, 1962; BOWEN and INMAN, 1971; GREENWOOD and DAVIDSON-ARNOTT, 1979; GOLDSMITH *et al.*, 1982; HOLMAN and SALLENGER, 1986).

Aerial photographs, satellite images (SPOT 1) and accurate bathymetric surveys, respectively realized by the Institut Géographique National (I.G.N.), SPOT Image and the French Navy's Hydrography and Oceanography Branch (S.H.O.M.) show the common presence of a crescentic bar along the Aquitaine coast, a sandy coast 230 km long between Gironde and Adour estuary in the Gulf of Biscaye. A part of a SPOT image (channel XS1, 500-590 nm) showing this submarine crescentic bar is presented in Figure 1 (Date: 9 May 1987. Coordinates: between 44°40′ and 44°45′N–1°10′ and 1°20′W). The distances between the horns are variable—between 1000 and 500 m—and the distance between the coast and the farthest part is about 450 m.

In this area, numerous aerial photographs show the undulation of wave crests. An example is given in Figure 2 (Date: 1977. Coordinates: 45°06′N and 1°11′W). The wave lengths (about 600 m) of these undulations are comparable with distances between crescentic horns.

The aim of this paper is to show that the refraction of waves on a crescentic bar can induce this coastal undulation of wave crests.

89025 received 17 April 1989; accepted in revision 23 February 1990.

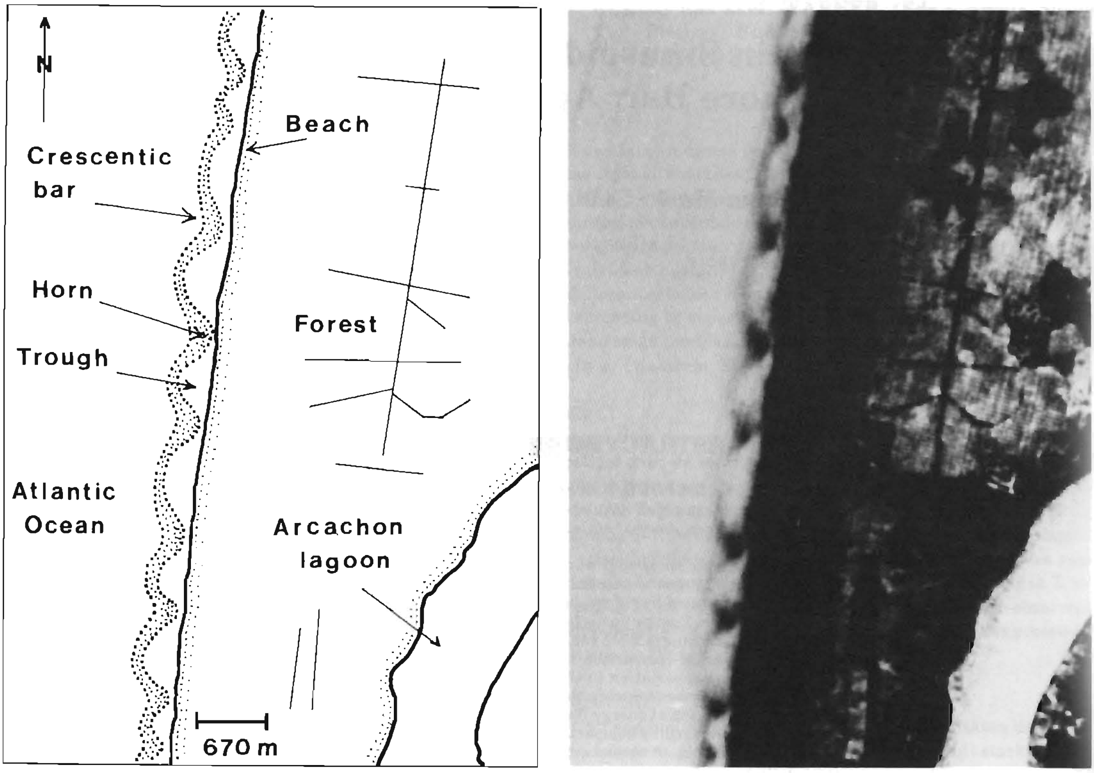

Figure 1. Line drawing (a) made from spot image (XS1 band), (b) displaying the submarine crescentic bar (SPOT 1, 9 May 1987, 44°48'N 1°15'W). Dimension of this area: 3300 x 2800 m.

First, this paper presents the characteristics of a computer program to model the refraction of a sinusoidal wave with an essay on a typical bathymetry. Secondly, this program is applied to the continental shelf of Aquitaine to determine the incidence of wave crests at a depth of 15 m. This preliminary study makes it possible to approach a second stage, that is refraction over the nearshore slope and stretching from a depth of 15 meters to the surf zone. Finally, the undulation of wave crests and the energy variations are analyzed during high, mid and low tide.

REFRACTION PROGRAM CHARACTERISTICS

All methods of refraction analysis are based on Snell's and Descartes's refraction laws relating to the refraction light. The assumptions made are: wave energy between wave rays or orthogonals remains constant; waves are small amplitude and monochromatic; effects of currents, winds, diffraction and reflection are considered negligible. The linear and small amplitude wave has been chosen because it's easy to verify the processing results.

General Equations Used

The wave celerity and wavelength decrease with depth:

$L = CT \qquad C = [(gL/2\pi)\tanh(2\pi d/L)]^{1/2}$

d = depth, C = wave celerity, L = wavelength, g = gravity, T = period

The velocity of a wave group Cg is given by:

$Cg = nC \qquad n = 1/2[1 + (4\pi d/L) / (\sinh(4\pi d/L))]$

The wave energy E is the sum of its kinetic energy (Ek) and its potential energy (Ep):

$E = Ek + Ep = \rho g H^2 L/8 \qquad \rho$ = mass density of water

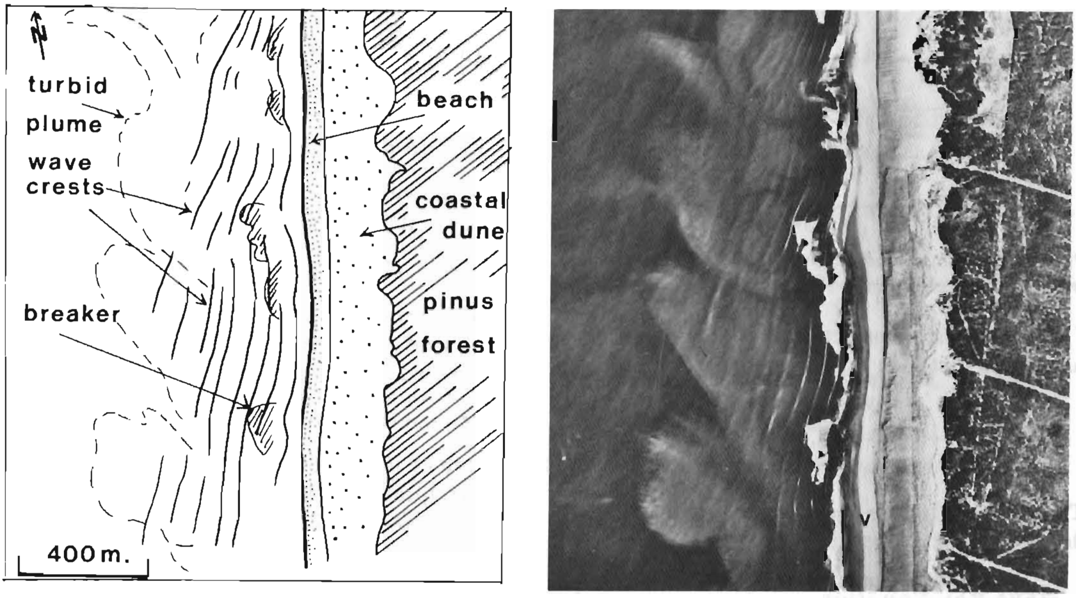

Figure 2. Line drawing (a) made from aerial photograph, (b) showing the undulation of wave crests near the coast (I.G.N., 1977, 45°06 N 1° 11′ W). Dimension of this area: 2100 x 1800 m.

H = Height = vertical distance between crest and trough.

Specific energy or energy density is given by the following relation:

$Es = \rho g.Hb^{2/8}$ (Hb = Height just before breaking)

The rate at which energy is being transported per unit crest width toward shore is the energy flux (Ft):

$Ft = Es.Cg \quad Cg = C$ in shallow water.

From the linear theory, when the wave crest makes an angle α with the shoreline, the energy flux of the longshore component (Fl) per unit length of beach is:

$Fl = Ft/2 \ . \ \sin 2\alpha$ (*Shore Protection Manual,* 1984)

Water particles move in elliptical paths in shallow water and in circular paths in deep water. Orbits are closed. (In reality, particle orbits are not completely closed.) Experiences and theories show that the wave celerity in shallow water is given by

$$C = [g\,(H + d)]^{1/2}$$

When the height (H) of the wave is not negligible in comparison with water depth, the true celerity diverges from the linear wave theory with a factor $(1 + H/d)^{1/2}$. The maximum ratio H/d before the breaking is about 0.8.

For the breaking threshold we use the Miche equation (MICHE, 1944):

$$(H/L)_{MAX} = 0.142 \tanh (2\pi d/L)$$

Computer Method

The program is based on an algorithm derived by MUNK and ARTHUR (1951). It was established by LAZURE (1984) and completed by ourselves.

Depth Gradient Interpolation Using subscripts i and j as depth grid counters for x and y coordinates respectively, the depth gradient at a grid point (i,j) may be written as

$$(\delta d/\delta x)i,j = [d(i+1)j - d(i-j)j] / 2\Delta x$$

$$(\delta d/\delta y)i,j = [d(j+1)i - d(j-1)i] / 2\Delta y$$

Δx and Δy are the grid spacing along the x and y directions respectively. For determining the depth or the depth gradient for an arbitrary point within a grid, the following interpolation is used (Figure 3):

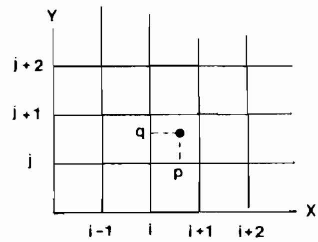

Figure 3. Depth gradient interpolation.

f = depth with respect to x and y; subscript p and q are distance ratio varying from 0 to 1.

$f(i+p)\ (j+q) = (1-p)\ (1-q)fi,j + p(1-q)f(i+1)j + q(1-p)fi,\ (j+1) + qpf(i+1),\ (j+1)$

The interpolation method for gradient and depth uses 12 adjacent points.

Wave Ray Equation

A monochromatic wave moves with a celerity C. The distance along the wave front and between 2 rays R1, R2 is df. The wave ray R1 will move a distance ds for a time increment dt according to

$ds = Cdt.$

On R2 we have : $ds' = (C+dc)dt$.
By geometrical construction (Figure 4) and if A = the angle between the wave ray and the X axis, we obtain:

$dcdt = -dA.df$

$dA/dt = -dc/df \quad (1)$

$dA/dt = (dA/ds)\ .\ (ds/dt) = C.\ (dA/ds)$
$k = dA/ds \quad dA/dt = C.k \quad (2)$

k = ray curvature. By introducing equ. (1) into equ. (2) it's obtained:

$k = -\ (1/C)\ .\ (dc/df)$

The relationship between the celerity gradient (dc) and the depth gradient (dd) may be expressed by:

$kc = -(1/C)\ .\ (dd/df)\ .\ (dc/dd)$

where kc is defined as the curvature coefficient. Consequently, the ray curvature k may be determined from the curvature coefficient kc and

$k = kc.dd/df \quad (3)$

The ray curvature coefficient kc for small amplitude waves is:

$kc = (1-2n)\ /2nd$
$n = 1/2[1 + (4\pi d/L)/(\sinh(4\pi d/L))]$

Celerity computation and curvature coefficient are obtained by the Raphson-Newton method. The procedure is repeated up to have a very small difference (0.001) between two iteration. When the point n+1 is positioned, the height is computed.

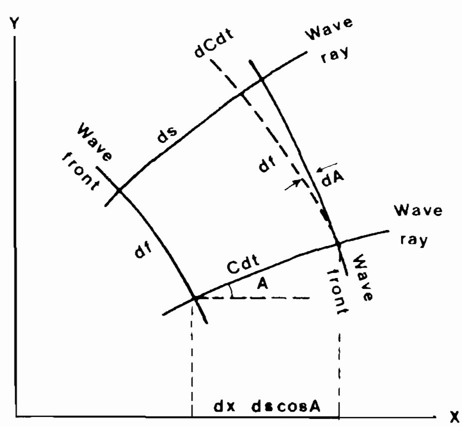

Figure 4. Wave rays (orthogonals) construction.

Wave Height Equation

The change in the wave height is calculated from the condition that the rate of wave energy is constant between 2 adjacent rays. In shallow water:

$$H/H0 = (Cg0/Cg)^{1/2}.(b0/b)^{1/2}.kf$$

b0 = distance between 2 rays in deep water, b = distance in shallow water. kf = friction coefficient.

$$(Cg0/Cg)^{1/2} = ks \qquad (b0/b)^{1/2} = kr$$

ks = shoalling coefficient.
Generally the linear wave theory over estimates the increasing of height just before the breaking. The height is computed at each time increment. The drawing is stopped when the breaking according to the Miche equation is reached or if the refraction coefficient is about $kr \geqslant 2$.

Energy Flux and Longshore Component

It's computed in Megajoule/hour and per unit length of beach (m):

$$Ft = [\rho g\,(Hb^2)/8\ .\ C\ .\ 3600]\ .\ 10^{-6}$$

$\rho g = 10050$. Hb = height just before breaking. C = Cg in shallow water

1 h = 3600 s, 1 megajoule = 10^6 joule.

The longshore energy flux is computed according to the variation of α angle, from the isobathe under the breaking zone. The variations of α were measured manually from the bathymetric plan.

Operation Procedure

To advance a point n with coordinates (xn,yn) along a wave ray to a point n+1 with coordinates x(n+1), y(n+1) the following equations are used:

$$A = An + 1/4\,(kn + k(n+1))Dn$$

k = the ray curvature given in equ. 3

D = incremental distance along a ray

A = angle between the ray and the x axis.

$$X(n+1) = Xn + Dn.\cos A$$

$$Y(n+1) = Yn + Dn.\sin A$$

$Dn = [\ (Cn + C(n+1)\ /\ 2].\Delta t$ $\quad \Delta t$ = time increment

For the first iteration, $k(n+1) = kn$ and $C(n+1) = Cn$

Programation steps (Program written in Fortran 77)

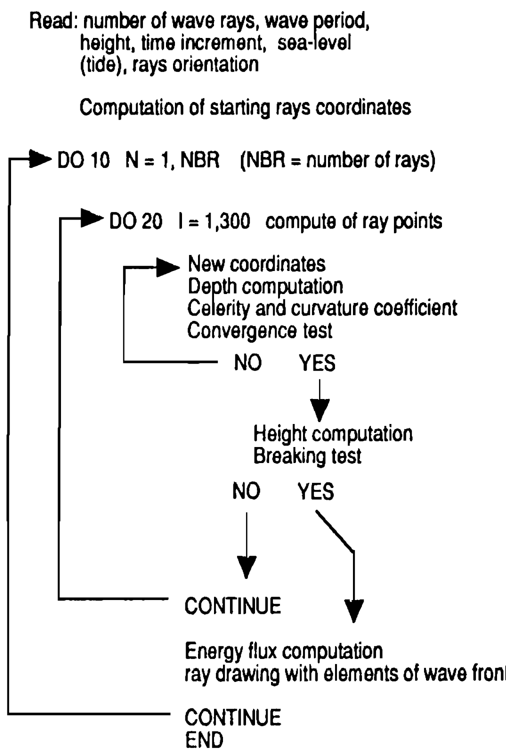

(The depths grid is recorded before the program running.)

Test of the Model To test the model, an idealized shelf with a submarine valley and a submarine ridge was used (Figure 5). The depths were recorded on an 18 x 23 matrix in squares of 500 x 500 m. The program was tested with a 10 s period of waves propagating toward the shore. The water depth at the initial position is 80 m and the wave height 4 m. The resulting refraction diagram is shown in Figure 6. This experience gives a relative good corre-

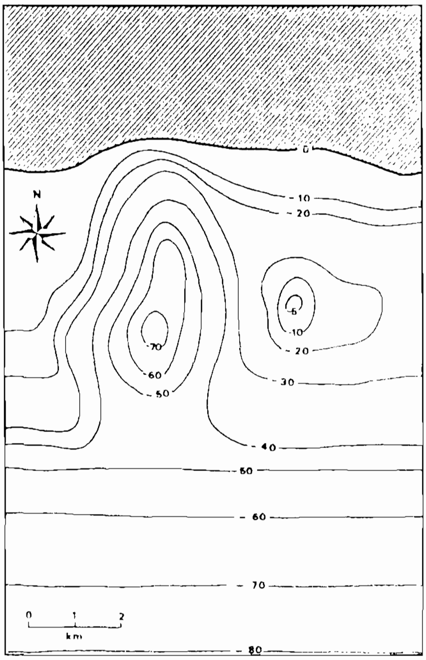

Figure 5. Typical morphology used to test the refraction program.

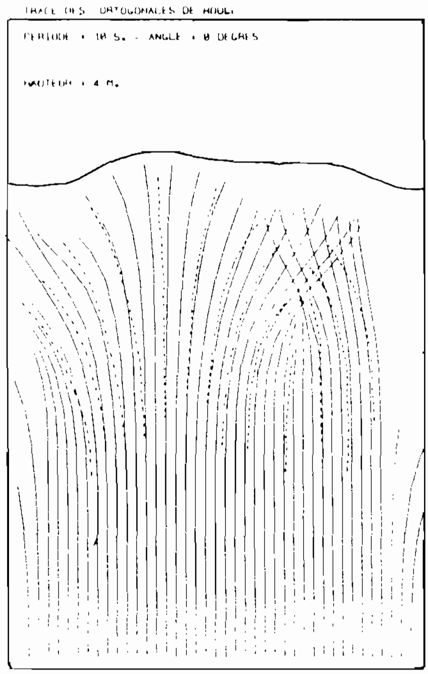

Figure 6. Refraction diagram obtained from Figure 5 bottom topography. In hatch, orthogonals manually drawn.

lation with orthogonals drawn from manual method represented in dashed lines. The shoal tends to focus wave action. The orthogonals are more closely spaced. Since the wave energy contained between two rays is constant, the energy is focused (b0/b > 1.0) and the waves are higher than they would be if no refraction occurred. Conversely, a submarine depression causes rays to diverge (b0/b< 1.0), resulting in low heights at the shore.

WAVE REFRACTION ON THE AQUITAINE CONTINENTAL SHELF

The slope of the Aquitaine continental shelf off Cap-Ferret is gentle. The depth of 100 m is reached 34 km offshore, giving an average slope of 3/1000. This shelf has no important irregularities and is covered by quartz sand and, to a lesser extent, by gravel (CASTAING, 1981; FROIDEFOND, 1985). South of Cap-Ferret the extensive seaward opening of the Arcachon Bay interrupts this sandy coastline.

This one is dominated by a high energy wave regime. Storm wave heights more than 10 m are not uncommon. We have analyzed the wave-rider buoy (above−30 m depth) data recorded during the year 1987 by the Centre d'Essai des Landes (C.E.L.). The average data are given in the Tables 1 and 2. (17 days without records).

But these data are twice averaged. For example, on the 28 of March 1987 the buoy has recorded one wave of 8.3 m height and 12 waves upper 6 m when the one-third highest wave (H1/3) is 4.1 m. The significant wave height averages (Σ H1/3) exceed 1 m for 60% of the time, 2 m for 19% of the time and 3 m for 5% of the time. The wave period averages (T1/3) exceed 8 s for 48% of the time, 10 s for 15% and 12 s for 3.5%, and westerly and northwesterly waves are the highest (PENIN, 1980). Loss of wave power through friction seaward of the breaker zone is unknown, but probably slight. Tides are semi-diurnal with an average spring tide range of 4.5 m.

Data from the dominant storm waves, with a deepwater direction of wave approach around 103°N and a period of 12 s, are selected for the refraction study. Figure 7 shows the refraction

Table 1. *Average height in m of the one-third highest waves (H 1/3) in 1987 (Average of 48 records (15 mn each) per day).*

Height 1/3	Number of days	%	Height 1/3	Number of days	%
0.00–0.25 m	0	0.0	0.25–0.50 m	20	5.7
0.50–0.75	71	20.4	0.75–1.00	49	14.1
1.00–1.25	53	15.2	1.25–1.50	34	9.8
1.50–1.75	35	10.1	1.75–2.00	21	6.0
2.00–2.25	22	6.3	2.25–2.50	7	2.0
2.50–2.75	14	4.0	2.75–3.00	6	1.7
3.00–3.25	7	2.0	3.25–3.50	2	0.6
3.50–3.75	3	0.9	3.75–4.00	0	0.0
4.00–4.25	2	0.6	4.25–4.50	1	0.3
4.50–4.75	1	0.3	4.75–5.00	0	0.0

Table 2. *Average period in s of the one-third longest period (T 1/3) in 1987 (Average of 48 records per day).*

Period 1/3	Number of days	%	Period 1/3	Number of days	%
03.0–03.5 s	0	0.0	03.5–04.0 s	3	0.9
04.0–04.5	6	1.7	04.5–05.0	8	2.3
05.0–05.5	23	6.6	05.5–06.0	19	5.5
06.0–06.5	28	8.0	06.5–07.0	24	6.9
07.0–07.5	34	9.8	07.5–08.0	37	10.6
08.0–08.5	35	10.1	08.5–09.0	30	8.6
09.0–09.5	22	6.3	09.5–10.0	26	7.5
10.0–10.5	14	4.0	10.5–11.0	9	2.6
11.0–11.5	10	2.9	11.5–12.0	8	2.3
12.0–12.5	4	1.1	12.5–13.0	6	1.7
13.0–13.5	0	0.0	13.5–14.0	2	0.6

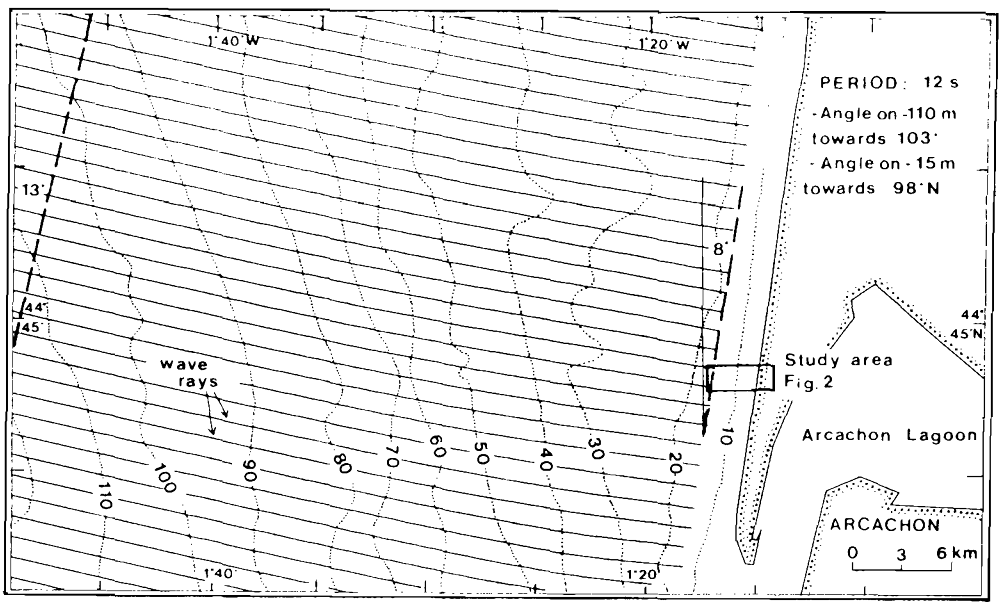

Figure 7. Refraction diagram of a sinusoidal wave directed towards N 103°E and with a period of 12 s on the central part of the Aquitaine continental shelf.

of these waves. Bottom contours appear as dotted lines and the orthogonals to the crests as continuous lines. Offshore from the crescentic bar the orthogonals turn progressively towards 98° at a depth of 15 m (44°43'N–1°15'W, framed on Figure 7). The incidence of the orthogonals is then 98 N. Wave crests are then 8-188°, parallel to the coast.

REFRACTION ON A CRESCENTIC BAR

Physical Environment

The nearshore zone (Figure 8) is covered mainly by quartz sand with a grain size between 0.25 and 0.5 mm. This sand is generally set in motion in water depth up to 12 m (wave height < 2 m) (ORGERON, 1973). The crest of the crescentic bar is approximately 500 m from the beach (Bathymetric Chart, S.H.O.M. 1967; FROIDEFOND, 1985). It is separated from the beach by troughs reaching a depth of 7 m and arranged at regular intervals along the coast. These troughs are separated from each other by horns. The crescentic bar is situated further away from the shore, and is deeper in front of the trough (Figure 9). Several aerial photographs (I.G.N. 1977-1982-1984-1985) show the great variability of these forms that probably develop around a profile of equilibrium (GREENWOOD and MITTLER, 1984). From BATTJES equation (1974) and the studies of WRIGHT *et al.* (1986) we consider that wave reflexion is a secondary parameter along this coast. Indeed, the average slope between −10 m and 0 m is gentle—1.5:100—and the maximum slope just in front of the bar crest is about 5:100. It is dominantly a dissipative open coast beach.

On aerial photographs wave crests are easily observed and show undulations such as those illustrated in Figure 2. To determine if refraction is the cause of these undulations, we have extended the computation into the nearshore and the computation of energy flux and its longshore component over the crescentic bar. The energy flux in the surf zone is approximated by assuming conservation of energy in the shoaling waves, using Airy (linear) wave theory and then calculating the energy flux in relation to the breaker position. The energy flux per unit length of wave crest (Ef) and the energy flux in the direction of wave propagation per unit length of beach are calculated from different angle values measured between the isobathe under the breaking zone and wave crest.

In the computer algorithm, wave propagation stops when the breaking coefficient according to MICHE's equation (1944) is reached. In the computation of wave height we have not integrated the friction factor because of lack of data. Consequently, the results relating to energy are overestimated, but as the area studied has an almost homogenous sandy topography, the error may be considered as constant, at least in first approximation. The refraction dia-

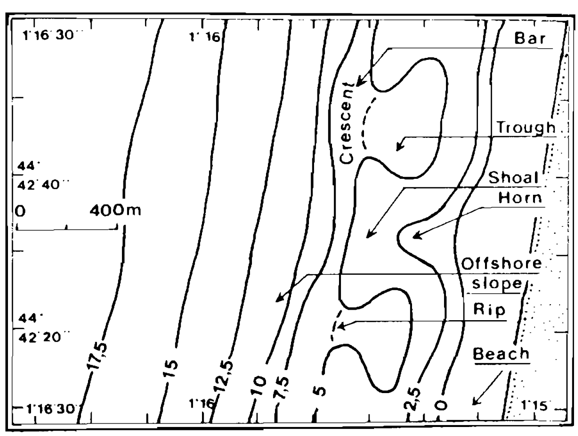

Figure 8. Bathymetric chart of the nearshore zone, established from S.H.O.M. n°13-3-49 (1967, 1/10000) plotting sheet.

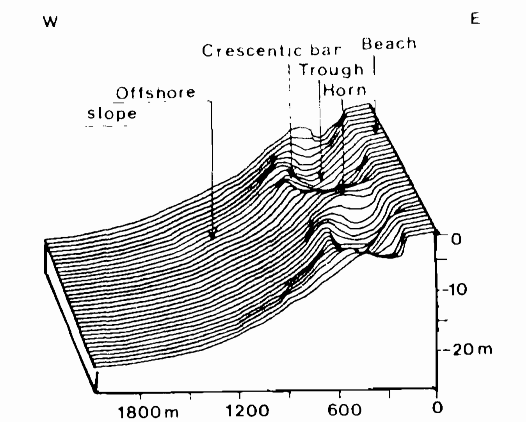

Figure 9. Block diagram of this nearshore zone from the bathymetric chart.

grams were constructed from bottom topography larger than the part illustrated in Figure 8 (matrix of 34 x 20 squares of 150 x 150 m) and Figure 10. We chose the most demonstrative part of this crescentic bar to visualize the effects of refraction in terms of tide variations.

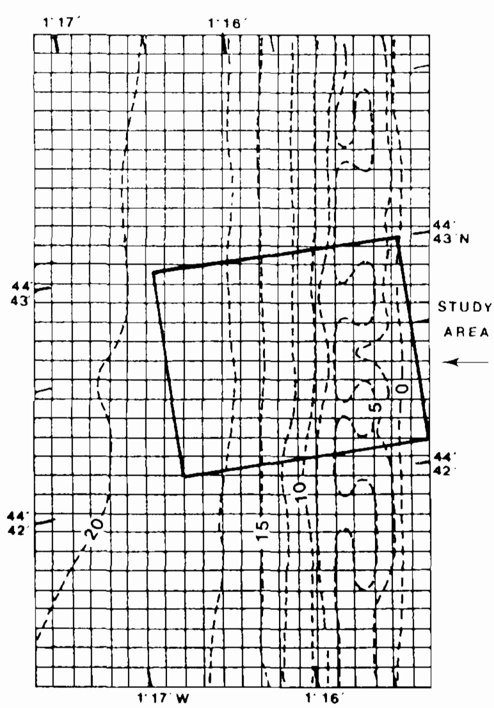

Figure 10. Matrix of depths used to construct the refraction diagrams.

Results

Different cases were examined in terms of tide and wave orientation.

Refraction at Low Tide

In Figure 11, we reproduce an example of wave refraction over the bathymetry of Figure 8 at low tide (1 m above the lowest tide) and with 3 m height, 12 second period waves. The wavelength (distance between two wave crests) decreases from about 154 m to 72 m just before the breakers. The angle of the breaking wave (α) is computed from the intersection of the $-$ 2.5 m depth contours (below the breakers) with the orthogonals. The observed divergence of the orthogonals in the troughs and convergence on the horns (shoal area) involve an undulation of wave crests similar to that in Figure 2. A divergence corresponds to a decrease in energy flux per unit of wave crest (250-350 Mj/hr) and conversely, a convergence causes an increase in flux (400–500 Mj/hr)–see Figure 11, curve A. As a consequence, the latter produces a greater steepness and breaking than in a trough.

A small part of this energy initiates the longshore current. It is the angular change between the crests of waves and the $-$ 2.5 m contour which is critical. The longshore current would be directed simultaneously to the north ($-$) and to the south ($+$). These variations (in Figure 11), shown by small arrows, emphasize the starting of the rip-current from the center of each trough. The energy of the longshore component goes from a minimum opposite troughs and ridges (0–10 Mj/hr) to a maximum in the intermediate parts (150–200 Mj/hr)–see curve B on Figure 11.

Refraction at Mid Tide

The refraction at midtide, that is to say, at 2.5 m above the lowest tide, has been studied in the same conditions as the precedent. The angles of the breaking wave (α) are measured from the intersection of the $-$ 3.5 m depth contours with the orthogonals. Results (Figure 12) are not very different that the precedent. The energy of

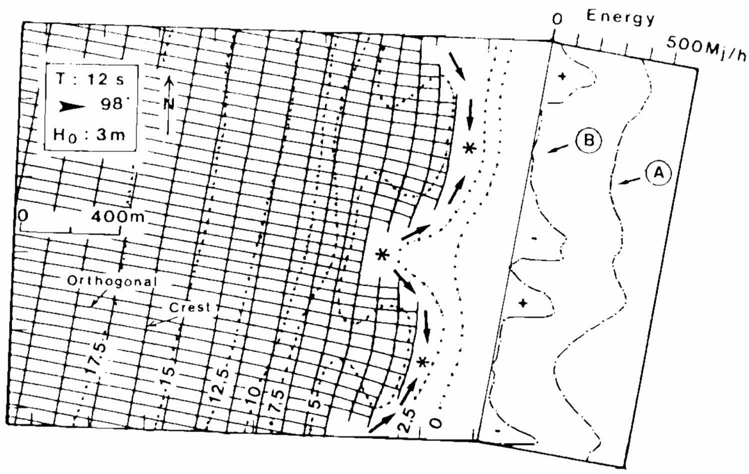

Figure 11. Refraction diagram for a sinusoidal wave directed towards N 98°E at a depth of 15 m, with a period of 12 s, a height of 3 m and the wave crests. Sea level: + 1 m above lowest tides. To the right, the curves of the energy flux in Mj/hr and per unit length of wave crest, and the longshore component in Mj/hr per unit length of beach parallel to the − 2.5 m depth contour. Arrows indicate the probable orientation and gradient of longshore currents.

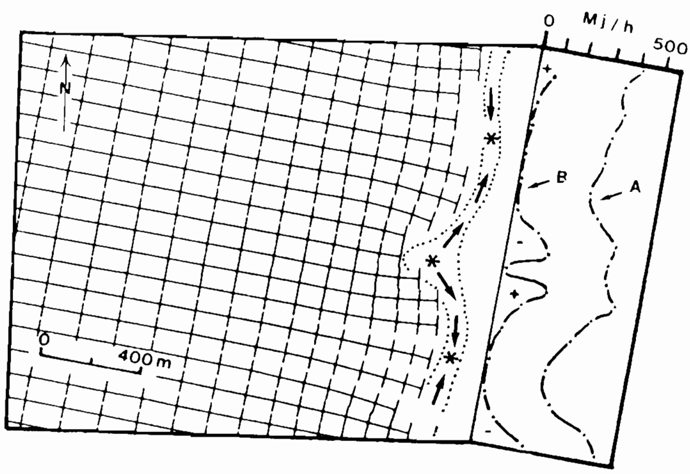

Figure 12. Refraction diagram for waves similar to the above (T = 12 s, H0 = 3 m, direction of orthogonals: N 98°E) but at mid-tide.

the longshore component has slightly decreased (curve B on Figure 12) by comparison with low tide (Figure 11).

Refraction at High Tide

Figure 13 shows a wave refraction diagram similar to the previous cases, but at high tide (4.5 m above the lowest tides). The angle of breaking waves is deduced from the intersection between the + 1.5 m contour and the orthogonals. The breaking zone, from the computation of Miche's equation, has advanced towards the backshore. Zones of wave convergence and divergence are not laterally displaced. The variation in energy flux is nearly

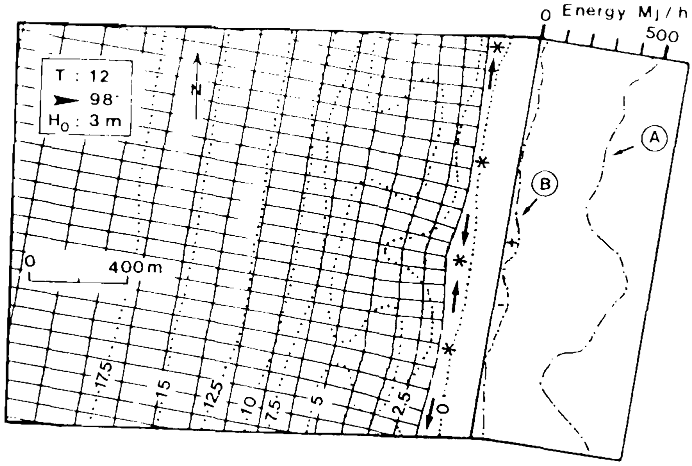

Figure 13. Refraction diagram for waves similar to the precedent (T = 12 s, H0 = 3 m, waves directed N 98°E), but with sea level at + 4.5 m (high tide) above the lowest tides. In this diagram the longshore currents would converge on horns.

identical to the flux computed at low tide (Figure 11). On the other hand, the longshore component of energy flux undergoes an important variation from low to high tide. Its orientation is inversed and the gradient lower. This variation is explained by the changes in bathymetry encountered by the propagation of waves due to the displacement of sea level from low to high tide. The variations of wave heights are visualized in Figure 14. As previous, the waves are higher on the horns than on the troughs.

Refraction With Oblique Waves

The orientation of oblique waves is chosen from data given by PENIN (1980): angle between wave crests and coastline = 20° (orthogonals: N 118°E). Refraction diagram (Figure 15) at low tide shows distinct differences by comparison with the precedent diagram (Figure 11). The cyclic variations of total energy flux decreases and the longshore component flux increases. One observes the dimi-

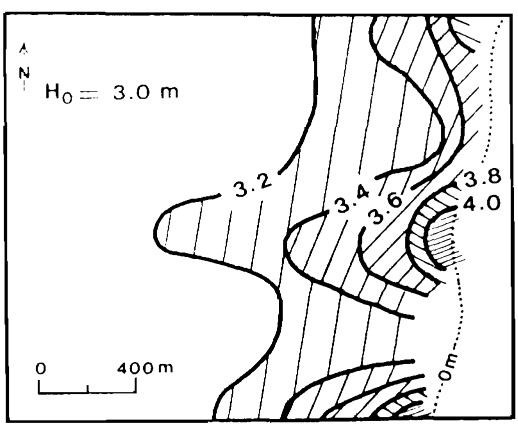

Figure 14. Variations of height waves for a refraction diagram at high tide (T = 12 s, H0 = 3 m, tide level = 4.5 m above the lowest tide level, direction of orthogonals: N 98°E).

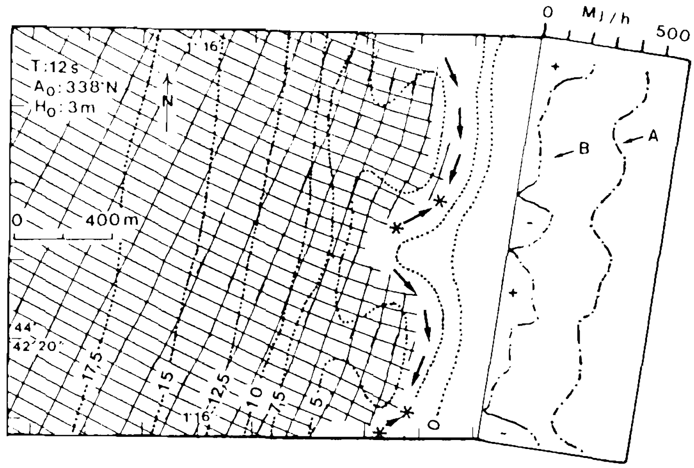

Figure 15. Refraction diagram for an oblique wave (T = 12 s, H0 = 3 m, direction of orthogonals: N 118°E) and at mid-tide.

nution of the northern longshore component with regard to south component. This one is dominant, but an inversion of the longshore component subsists on the northern edges of the horns.

The smoothing of the bar with diparition of the horns by oblique waves probably allows the installation of a continuous longshore current.

DISCUSSION AND CONCLUSION

The major explanation is to use the monochromatic sinusoidal wave theory in an irregular wave field, where wave breaking occurs probably with the presence of secondary waves such as seaward propagating long waves and edge waves (BOWEN and INMAN, 1971; AAGAARD, 1988). It is a complex area with many parameters and the refraction is a component from each other. Consequently the use of Battjes surf similarity parameter needs to be treated with care because we have observed diffraction patterns and crossed waves on aerial photographs.

The principal results are the following:

(1) From the simple model used, when the waves are parallel to the coast, a crescentic bar causes an undulation of wave crests through refraction.

(2) The total energy flux is higher on the horns than in the troughs (saddle area) of the bar.

(3) Analysis of the longshore component of energy flux emphasizes the formation of circulation cells with a rip-current located in troughs at low tide (Figure 16A) and on ridges (horns) at high tide (Figure 16B). In other words, circulation cells are mobile and displaced in accordance with the tide.

(4) When the waves are oblique to the coast, the variations of energy flux and longshore component are different. Total energy flux are higher in front of features perpendicular to the orthogonals. The longshore component is inversed on a short distance. Rip-currents would be located between trough and horn (Figure 16C). With time, the oblique waves and the longshore currents induced by longshore component flux will erode the horns and a continuous longshore current will establish. But if the oblique waves act during a short time, the crescentic bar morphology will subsist and the displacement of sediments by longshore currents will be discontinuous. So, the presence of a crescentic bar can explain a sedimentary flux lower than in a case of a coast without a crescentic bar. This process completes and corrects the former results relating to the Aquitaine coast (MIGNIOT and LORIN, 1978; FROIDEFOND *et al.*, 1983).

Finally, we sought to analyze again aerial photographs to correlate wave crests and the bottom topography. An aerial photograph (Figure 17) shows the wave crest undulations on the

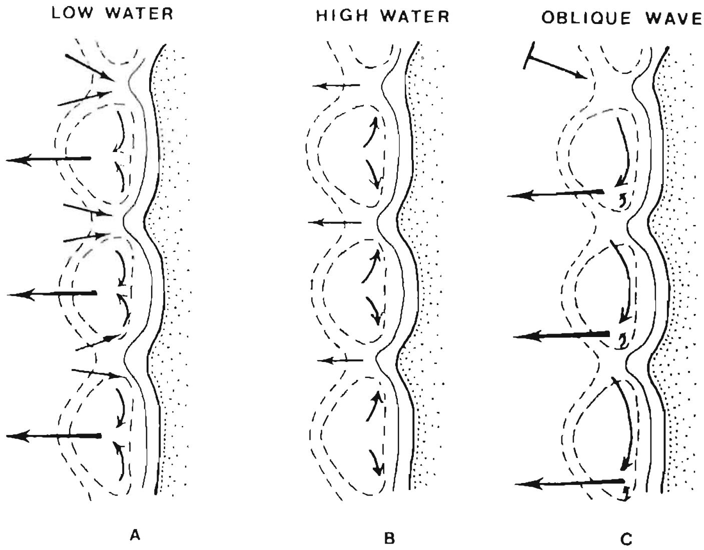

Figure 16. Current patterns (longshore and rip currents) deduced from the precedent diagrams for different cases: A = low tide, B = high tide, C = oblique waves.

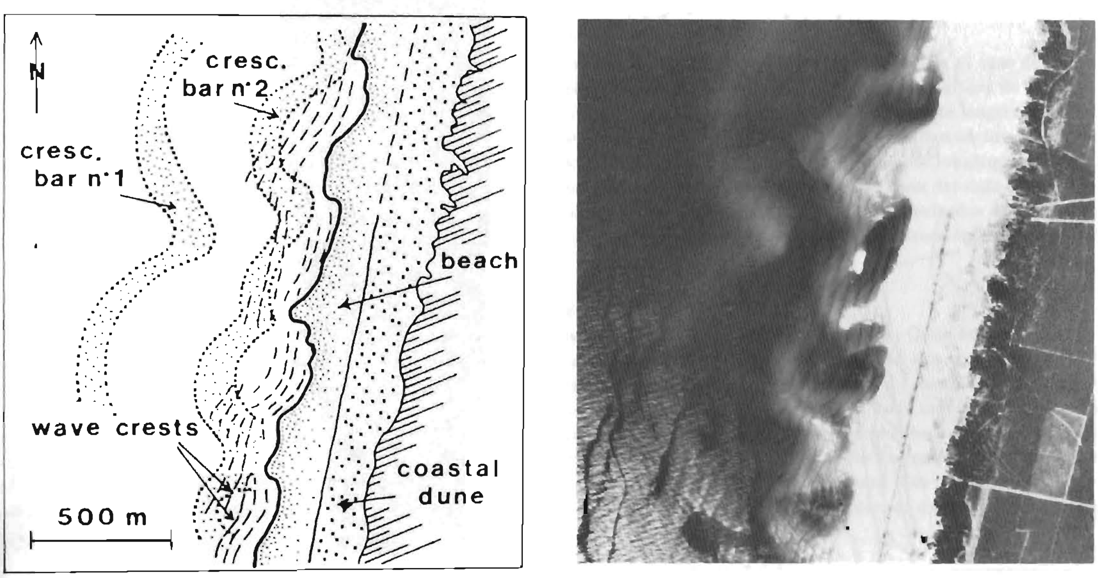

Figure 17. Simplified line drawing (a) and aerial photograph (b) showing a double crescentic bar and the undulation of wave crests (I.G.N., 1974, 44°06'N 1°19'30"W). Dimension of the area: 2500 x 2100 m.

troughs, but in a crescentic bar included in a larger crescentic bar. This double bar is a factor of complication (crossed waves, for example). Another aerial photograph (Figure 18) shows the foreshore morphology with cyclic banks separated by tidal channels called "baïnes" in this region. During the ebb, tidal currents are very strong and dangerous for bathers (several dead persons each year). These baïnes are the heads of the trip-currents and the bathers are carry offshore.

Moreover, sand displacement is accelerated in intertidal channels by tide and in nearshore zone by longshore currents and the suspensions are carried away under the form of turbid plumes (Figure 2).

So the use of remote sensing analysis associated with modelisation of wave refraction and energy flux variations permits a better knowledge of coastal sedimentary environments.

ACKNOWLEDGEMENTS

We are grateful for the assistance of P. Lazure and Dr. Salomon relating to the realization of the computer program. The manuscript was improved by constructive criticism from Prof. H. Lacombe (University of Paris) and Prof. B. Greenwood (University of Toronto). Finally, thanks are due to Prof. J. T. Moller, (Geologisk Institut, Aarhus Universitet), for his comments throughout the preparation of this paper.

LITERATURE CITED

AAGAARD, T., 1988. A study on nearshore bar dynamics in a low energy environment; Northern Zealand, Denmark. *Journal of Coastal Research,* 4, 115-128.

BARUSSEAU, J.P. and SAINT-GUILY, B., 1981. Disposition, caractères et formation des barres d'avant-côte festonnée du Golfe de Lion *Oceanologica Acta.* 4(3), 297-304.

BATTJES, J.A., 1944. Surf similarity. *Proceedings of the 14th coastal engineering conference,* Copenhague, pp. 466-480.

BOWEN, A.J. and INMAN, D.L., 1971. Edge waves and crescentic bars. *Journal of Geophysical Research.* 76, 8662-8671.

CASTAING, P., 1981. Le transfert à l'océan des sus-

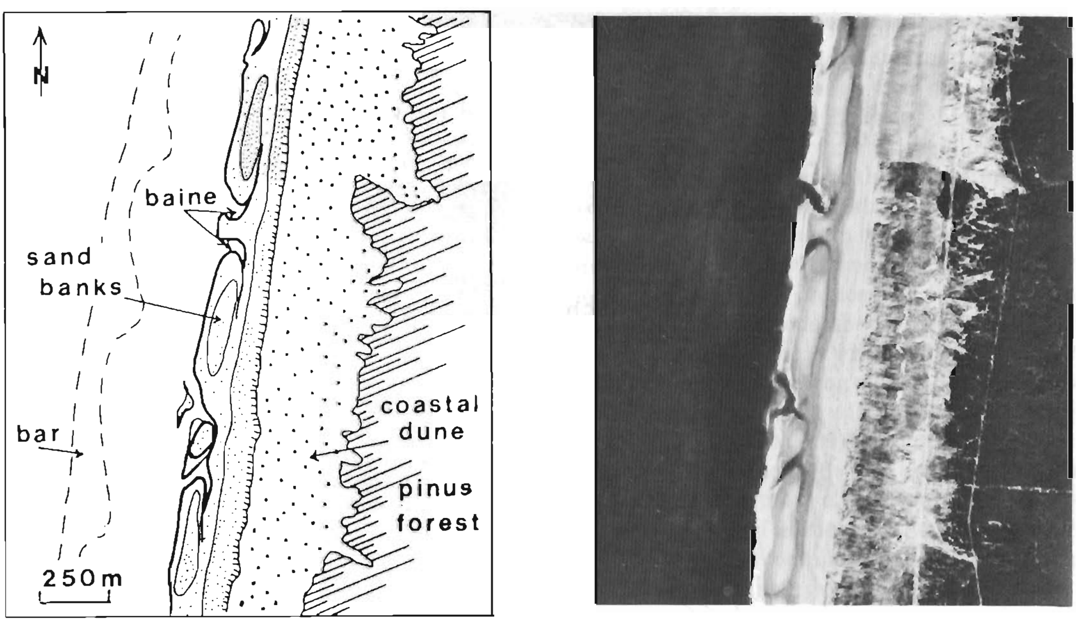

Figure 18. Line drawing showing cyclic repetition of banks and tidal channels on foreshore (a) from an aerial photograph (b) (I.G.N., 1973, 44°42'N 1°15'W). Dimension of the area: 2600 x 2200 m.

pensions estuariennes. Cas de la Gironde. Thèse d'Etat., *Université de Bordeaux I.* 530p.
CLOS-ARCEDUC, A., 1962. Algérie, Mission IGNF 12-14/250. Edition Technip. *Revue Photo-Interprétation* (Paris), 10(1), 5p.
Coastal Engineering Research Center, (C.E.R.C.), 1984. *Shore Protection Manual.* Washington: Department of the Army, vol. 1, 597p.
FROIDEFOND, J.M.; CASTAING, P., and WEBER, O., 1983. Evolution morphosédimentaire de la tête du canyon de Capbreton d'aprés les cartes de 1860 et de 1963. Utilisation des méthodes informatiques. *Bulletin Société Géologique de France (Paris),* XXV, (5), 705-714.
FROIDEFOND, J.M., 1985. *Méthode de géomorphologie côtière. Application à l'étude de l'évolution du littoral aquitain.* Mémoire Institut Géologie du Bassin d'Aquitaine (Bordeaux), 18, 273p.
GOLDSMITH, V.; BOWMAN, D., and KILEY, K., 1982. Sequential stage development of crescentic bars: Hahoterim Beach, Southeastern Mediterranean. *Journal of Sedimentary Petrology,* 52(1), 233-249.
GREENWOOD, B., and MITTLER, P.R., 1984. Sediment flux and equilibrium slopes in a barred nearshore. *Marine Geology,* 60, 79-98.
HOLMAN, R.A. and SALLENGER, A. H., 1986. High-energy nearshore processes. EOS, 67(49), 1369-1371.
HOM-MA, M. and SONU, C., 1963. Rythmic patterns of longshore bars related to sediment characteristics. *Proceedings of the 8th Coastal Engineering Conference,* A.S.C.E. (New York), pp. 248-278.
Institut Geographique National (I.G.N.), 1977 – *Missions de photographies aériennes:* Mission FR2889, n°2311. 1973 — Mission FR2434, n°214. 1974 — Mission 2574 n°882. 1982 — Mission IPLI 82200, n°26. 1984 — Mission 33 IFN 84 n°440. 1985 — Mission 300 1337, n°224.
LAZURE, P., 1984. *Etude de la propagation de la houle en zone littorale. Application au Golfe Normand-Breton.* Rapport de D.E.A., Université de Bretagne Occidentale, Brest, 39p.
MICHE, M., 1944. Mouvements ondulatoires de la mer en profondeur constante ou décroissante. *Annales des Ponts et Chaussées* (Paris), pp. 25-78.
MIGNIOT, C., and LORIN, J., 1978. Evolution du littoral de la côte des Landes et du Pays Basque au cours des dernières années. *In: Actes du Congrés de Bayonne 28-29 Octobre 1978,* Société des Sciences, Lettres et Art de Bayonne, pp. 629-661.
MUNK *et* ARTHUR, 1951. Wave intensity along a refracted ray. Circular n°521, *National Bureau of Standards,* Washington.
ORGERON, C., 1973. Sédimentologie des passes d'entrée du Bassin d'Arcachon. *Bulletin Institut Géologie du Bassin d'Aquitaine,* 15, 31-51.
PENIN, F., 1980. *Le prisme littoral aquitain: histoire holocène et évolution récente des environnements morpho-sédimentaires.* Thèse 3me cycle, Bordeaux, n°1577, 129p.
Service Hydrographique et Océanographique de la Marine (S.H.O.M), 1967. *Minute de sonde* (Brest), n°13-3-49, 1/10,000me.
WRIGHT, L.D.; NIELSEN, P.; SHI, N.C., and LIST, J.H., 1986. Morphodynamics of a bar-trough surf zone. *Marine Geology,* 70, 251-285.

□ RESUMEN □

Se ha estudiado la refracción de ondas sinusoidales sobre una barra crescéntica en la costa de Aquitania. En el caso de ondas paralelas a la costa, esta barra, compuesta por senos y crestas periódicas inducen una variación síncrona de la altura de ola y del flujo de energía a lo largo de la costa. El flujo de energía es menor en los senos que en las crestas. La componente longitudinal del flujo de energía cambia más rápidamente que el flujo total. La distribución teórica de esta energía se analiza en función de la variación de la profundidad de agua debido a la marea. El resultado muestra una variación de la componente longitudinal y, por tanto, un desplazamiento de las células de circulación y de las corrientes de salida con la marea. El caso de onda incidiendo oblícuamente, la variación cíclica del flujo de energía decrece y la componente longitudinal crece. Estos resultados se comparan con fotografía aérea. Una segunda barra crescéntica y los canales de marea complican el proceso de la refracción.—*Department of Water Sciences, University of Cantabria, Santander, Spain.*

□ RÉSUMÉ □

La réfraction d'une houle sinusoïdale simple sur une barre en croissant de la côte Aquitaine est étudiée. Cette barre, composée d'une répétition cyclique de creux séparés par des seuils, induit une variation synchrone de la hauteur des houles et du flux d'énergie le long du littoral pour des crêtes de houle parallèles à la côte. La composante longitudinale du flux d'énergie change plus rapidement que le flux total. La distribution théorique de cette énergie est analysée en fonction de la marée. Les résultats montrent une variation de la composante longitudinale et ainsi un déplacement des cellules de circulation et des courants de retour au cours de la marée. Dans le cas de houles obliques, les variations cycliques du flux d'énergie s'estompent, par contre la composante longitudinale augments. Les courants de retour sont décalés par rapport à l'axe du croissant. Ces résultats sont comparés à des photographies aériennes. On observe une complication des processus naturels par la présence d'une seconde bar en croissant et de chenaux de marée.

□ ZUSAMMENFASSUNG □

Einfache, sinusförmige Wellenbrechung an einer anwachsenden Sandbank an der Aquitaine-Küste wurde untersucht. Im Falle von parallel zur Küste verlaufenden Wellen löst diese Barre, die aus einem zyklischen Wechsel von Mulden und Sätteln besteht, eine gleichzeitige Veränderung von Wellenhöhe und Energiefluß entlang der Küste aus. Der Energiefluß ist in den Mulden geringer als auf den Sätteln. Die küstenparallele Komponente des Energieflusses ändert sich schneller als der gesamte Energiefluß. Die theoretische Verteilung dieser Energie wird im Vergleich zur Wassertiefe untersucht, die sich mit den Gezeiten ändert. Die Ergebnisse lassen eine Veränderung der küstenparallelen Energiekomponente und somit eine Verlagerung der Zirkulationszellen

und der Rippströme mit dem Tidenverlauf erkennen. Im Falle von schräg zur Küste verlaufenden Wellen nimmt die zyklische Veränderung des Energieflusses ab und die küstenparallele Komponente zu. Die Rippströme sind im Vergleich zum vorherigen Fall ausgeglichener. Diese Ergebnisse werden mit Luftbildern verglichen. Eine zweite anwachsende Sandbank und Priele verkomplizieren den Prozess der Wellenbrechung.—*Helmut Brückner, Geographisches Institut, Universität Düsseldorf, F.R.G.*